

000  
001  
002  
003  
004  
005  
006  
007  
008  
009  
010  
011  
012  
013  
014  
015  
016  
017  
018  
019  
020  
021  
022  
023  
024  
025  
026  
027  
028  
029  
030  
031  
032  
033  
034  
035  
036  
037  
038  
039  
040  
041  
042  
043  
044  
045  
046  
047  
048  
049  
050  
051  
052  
053

054  
055  
056  
057  
058  
059  
060  
061  
062  
063  
064  
065  
066  
067  
068  
069  
070  
071  
072  
073  
074  
075  
076  
077  
078  
079  
080  
081  
082  
083  
084  
085  
086  
087  
088  
089  
090  
091  
092  
093  
094  
095  
096  
097  
098  
099  
100  
101  
102  
103  
104  
105  
106  
107

# Supplementary Material for Test-Time Training for Change Detection in Remote Sensing Images

Anonymous CVPR submission

Paper ID 11246

## Abstract

*In this supplementary material document, we provide additional implementation details of our Test-Time Training for Change Detection in Remote Sensing Images.*

## 1. Additional Details on PCC

Polynomial color correction has been originally used in device characterization. In CD, we adopt this concept to map pre-change color space to post-change color space so that resulting difference image  $\mathbf{I}_d$  is less sensitive to isolated radiometric changes in pre-change and post-change images. Suppose that, we have  $N$  color samples from the post-change image, the corresponding camera response  $i_1, i_2, i_3, \dots, i_b$  (where  $b$  is the total number of color bands) can be represented by a  $1 \times b$  vector  $\rho_n$  where  $n = 1, 2, 3, \dots, N$ . If only  $i_1, i_2, i_3, \dots, i_b$  values are utilized in  $\rho_n$ , the transformation between pre-change and post-change is a simple linear transformation. The idea of PCC is that vector  $\rho_n$  can be expanded by adding more terms (i.e.,  $i_1^2, i_2^2, i_3^2, \dots, i_n^2$ ), so that better results can be achieved.

### 1.1. If pre-change and post-change images have only three-bands (R, G, and B):

If the pre-change and post-change images have only three bands (i.e.,  $b = 3$ , and  $i_1=R, i_2=G, i_3=B$ ), we have following polynomial kernel function  $\rho$ :

$$\rho = [R, G, B, RB, RG, BG, R^2, G^2, B^2, RGB] \quad (1)$$

### 1.2. If pre-change and post-change images have four or more-bands

If pre-change and post-change images have four bands (i.e.,  $b = 4$ , and  $i_1=R, i_2=G, i_3=B, i_4=Y$ ), we have following polynomial kernel function  $\rho$ :

$$\rho = [R, G, B, Y, RG, RB, RY, GB, GY, BY, R^2, G^2, B^2, Y^2, RGB, RGY, RBY, GBY, RGY] \quad (2)$$

For pre-change and post-change images having more than four bands ( $b > 4$ ), we consider polynomial terms up to third order to construct the kernel function considering the computational complexity of PCC.

### 1.3. Additional PCC results on OSCD dataset.

Figure 1, shows additional qualitative results on PCC on OSCD dataset [3]. From the figure we can observe that how well the polynomial correction transforms pre-change image color space in to the post-change color space via polynomial regression. This procedure greatly reduces the isolated colorimetric changes between pre-change and post-change images. Therefore, the resulting difference image  $\mathbf{I}_d$  is less sensitive to the color shifts between pre-change and post-change images.

**Continue on next page...**

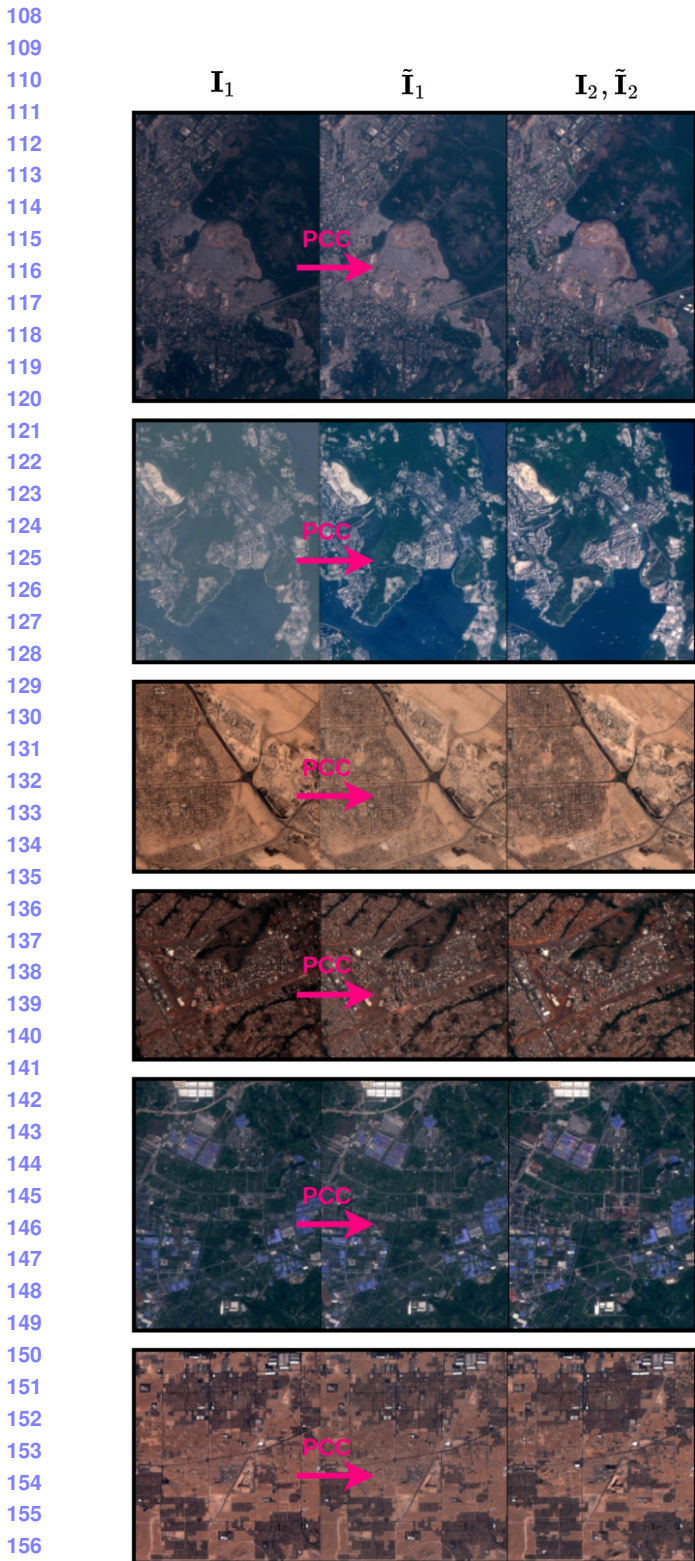


Figure 1. Additional qualitative examples on OSCD dataset [3] to illustrate how PCC maps pre-change image color space to post-change image color space using polynomial regression.



Figure 2. Additional qualitative examples on SZTAKI dataset [1, 2] to illustrate how PCC maps pre-change image color space to post-change image color space using polynomial regression.

216    **2. How our TTT-CD algorithm converges to  
217    optimum solution**  
218

219    Figure 3, 4, 5, 6, 7, and 8 depict given a pre-change and  
220    post-change image pair  $\{I_1, I_2\}$ , how our proposed TTT-  
221    CD algorithm finds the change probability map  $P_c$ . The  
222    TTT-CD algorithm takes difference image  $I_d$  as input and  
223    process it through a Deep-Change Probability Generator  
224    (D-CPG) to generate the change probability map  $P_c$ . The  
225    change probability map  $P_c$  is used to calculate the the pro-  
226    posed unsupervised loss for CD  $\mathcal{L}_{CD}$ . We iteratively min-  
227    imize  $\mathcal{L}_{CD}$  to find the optimal change probability map  $P_c^*$   
228    during the testing. Finally, we threshold  $P_c^*$  with an appro-  
229    priate probability value to obtain binary change map.  
230

231  
232  
233  
234  
235    **Continue on next page...**  
236  
237  
238  
239  
240  
241  
242  
243  
244  
245  
246  
247  
248  
249  
250  
251  
252  
253  
254  
255  
256  
257  
258  
259  
260  
261  
262  
263  
264  
265  
266  
267  
268  
269

270

271

272

273

274

275

276

277

278

279

280

281

282

283

284

285

286

287

288

289

290

291

292

293

294

295

296

297

298

299

300

301

302

303

304

305

306

307

308

309

310

311

312

313

314

315

316

317

318

319

320

321

322

323

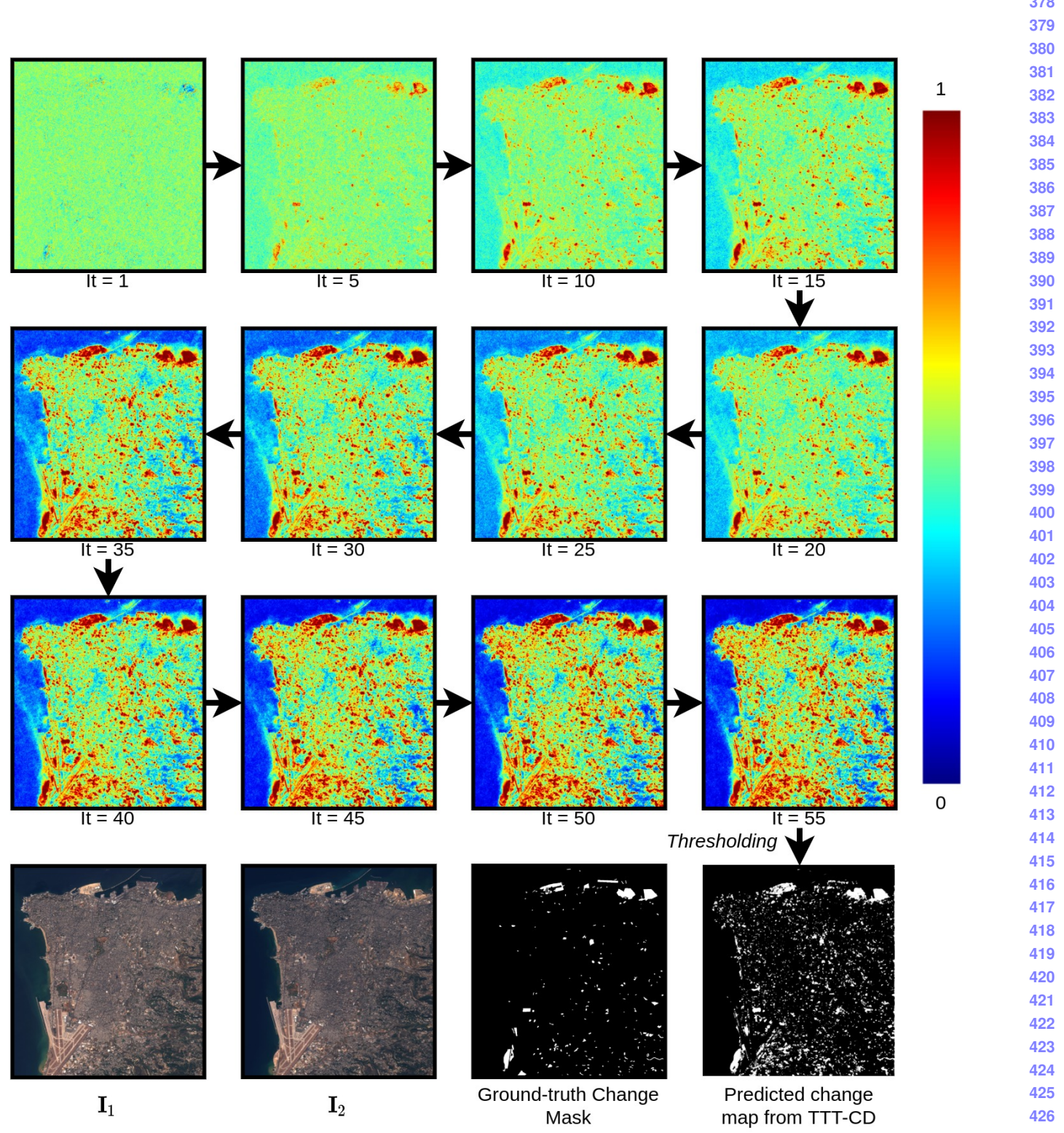


Figure 3. An example on beirut image in OSCD dataset.

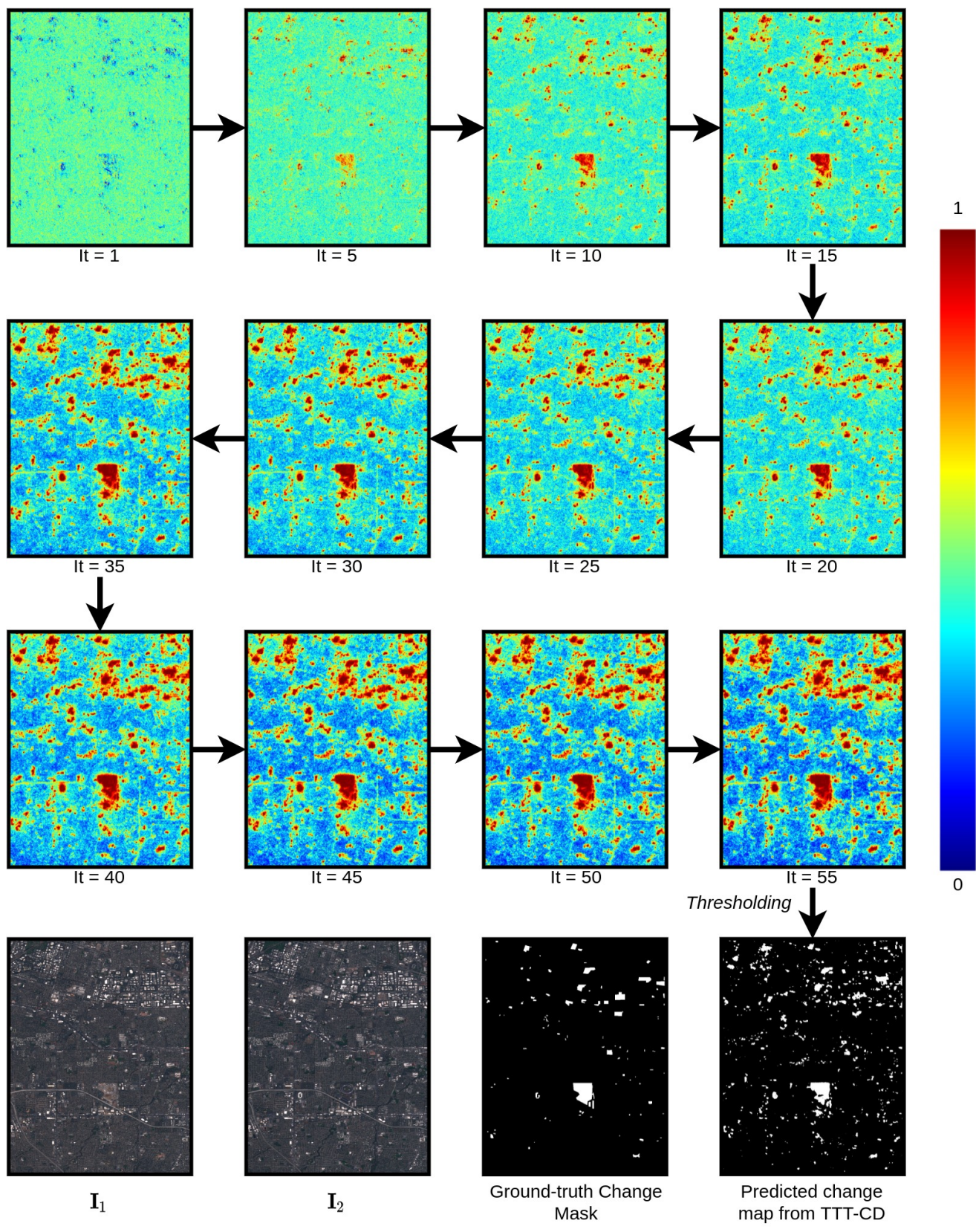


Figure 4. An example on cupertino image in OSCD dataset.

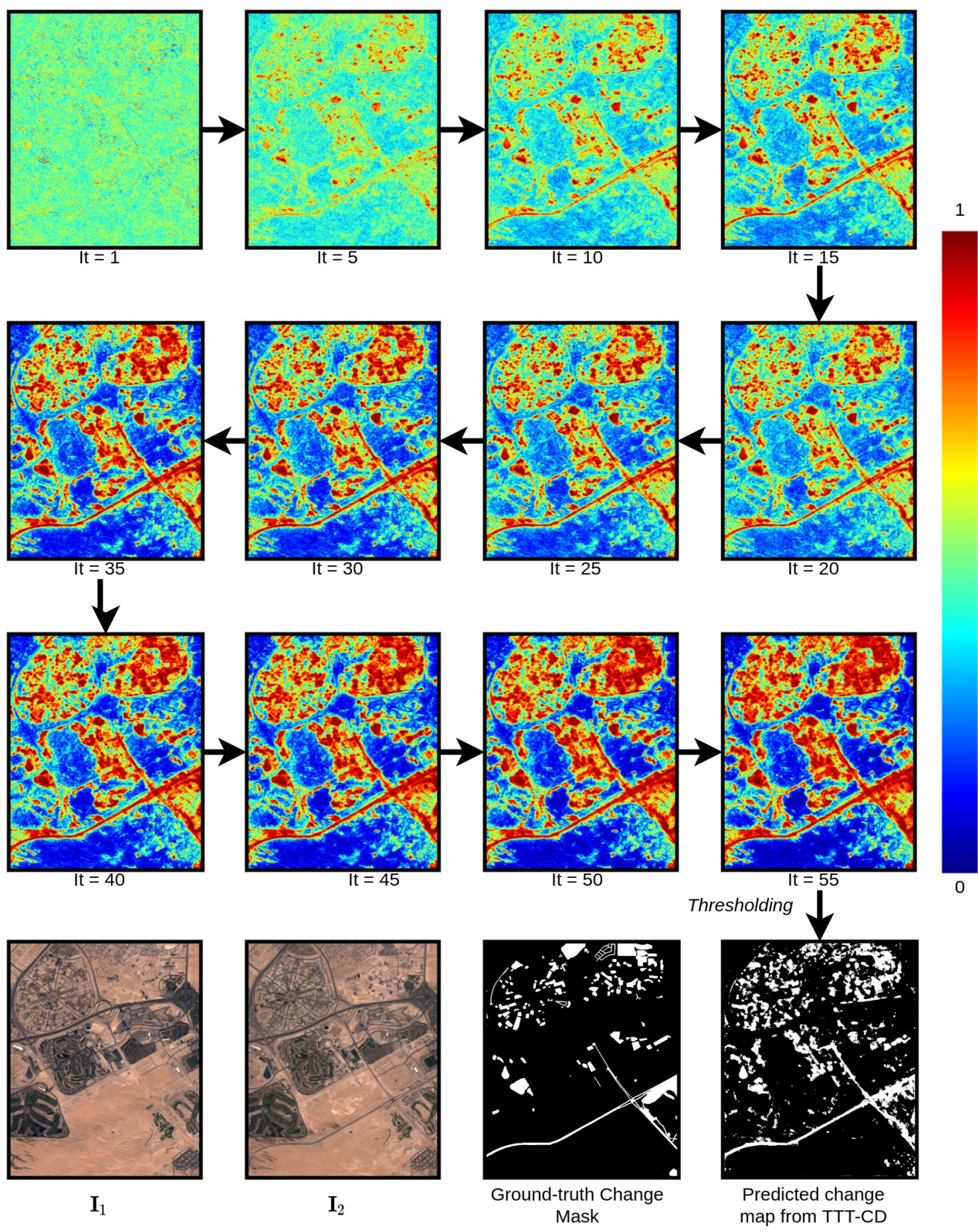


Figure 5. An example on cupertino image in OSCD dataset.

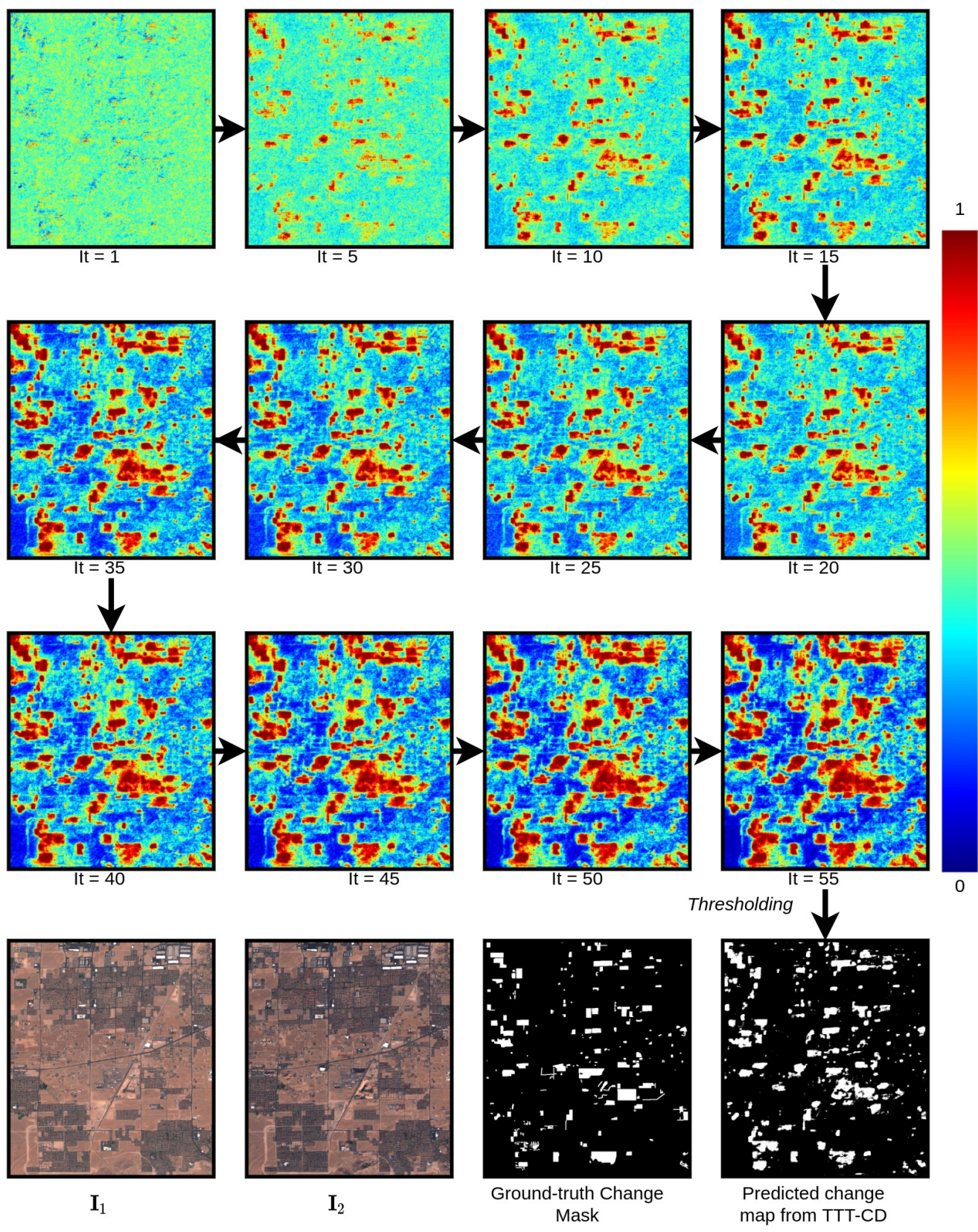
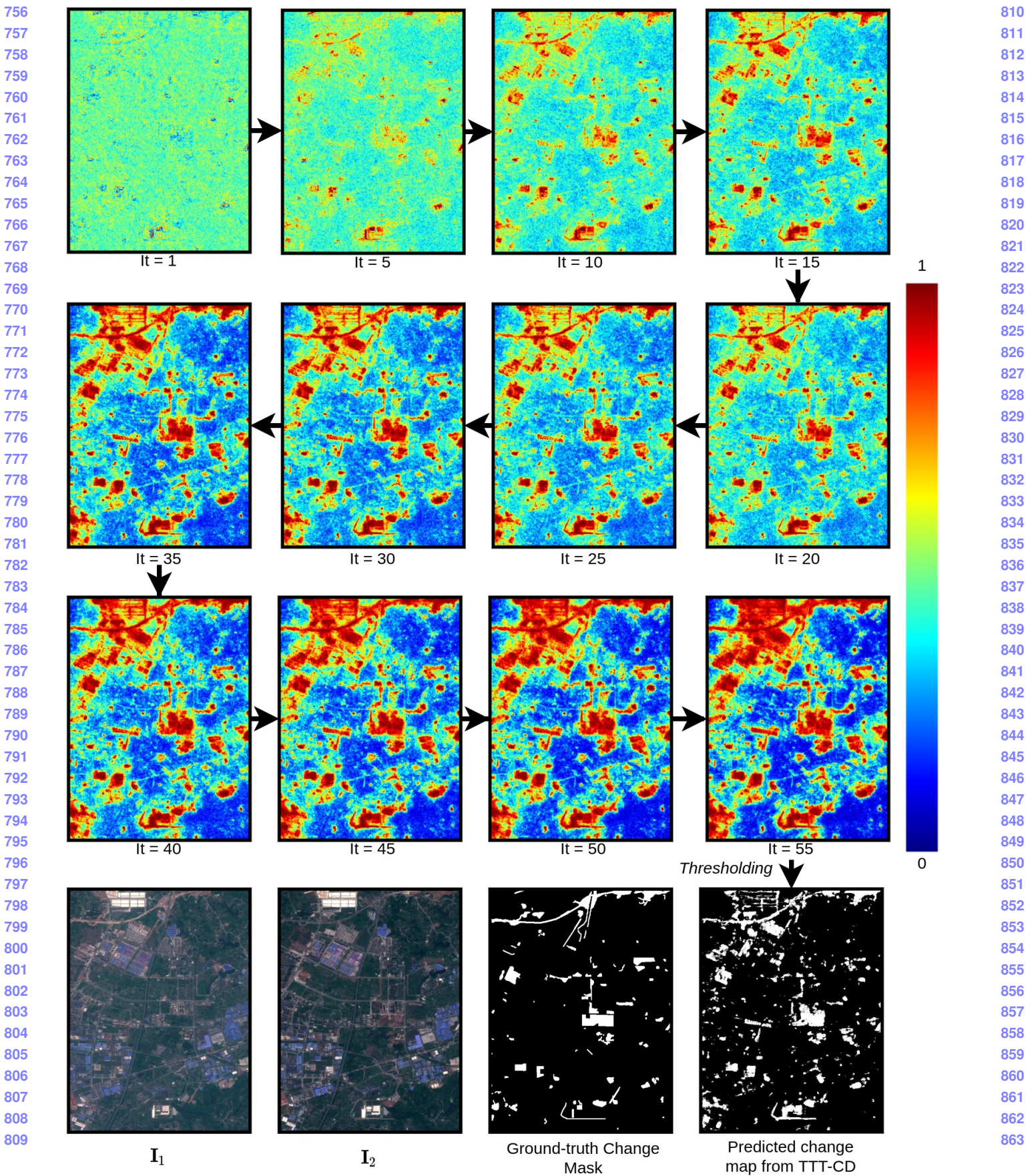


Figure 6. An example on lasvegas image in OSCD dataset.



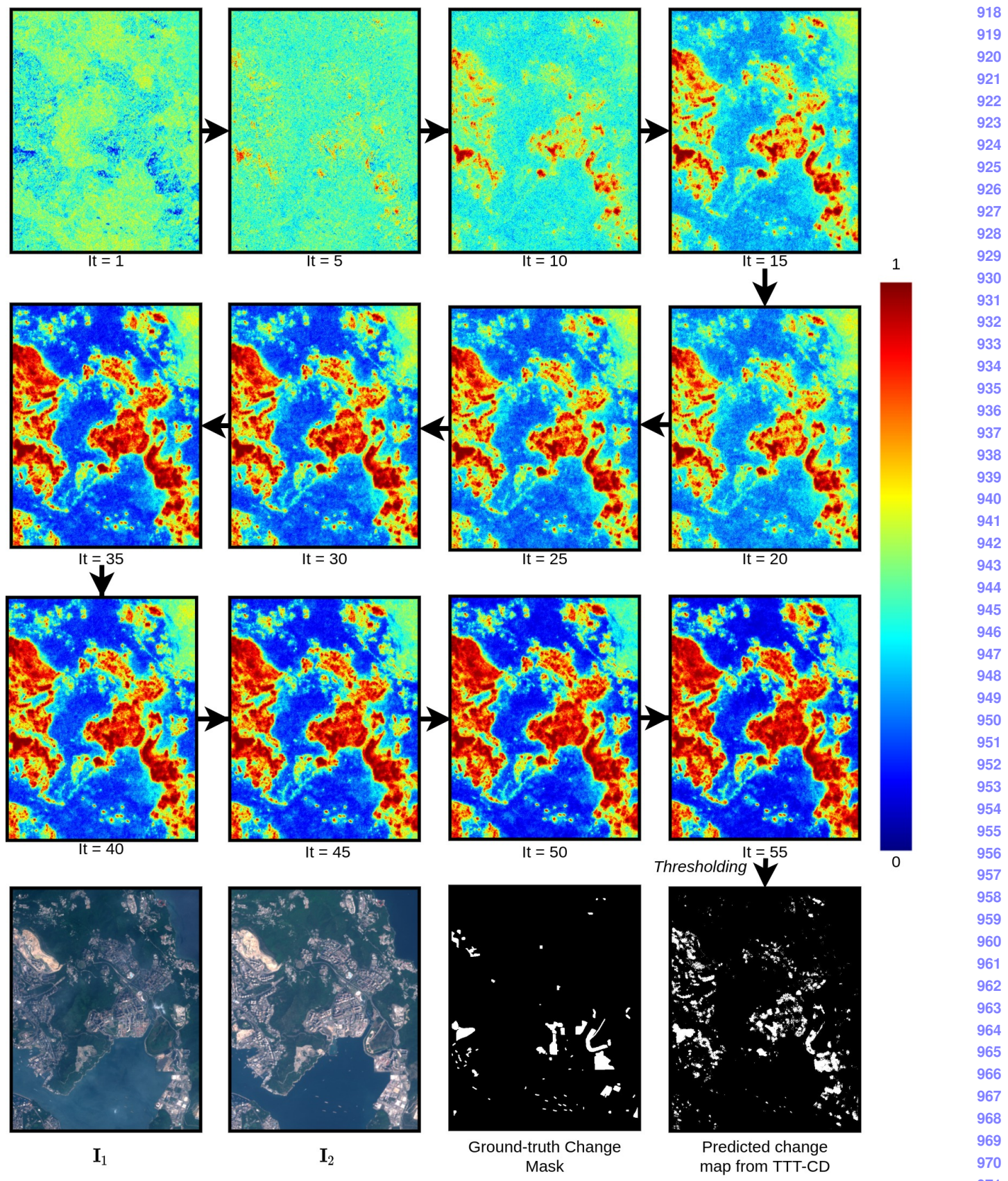


Figure 8. An example on hongkong image in OSCD dataset.

972	<b>3. Additional Qualitative Results on OSCD</b>	1026
973	<b>dataset</b>	1027
974		1028
975	Figure 9, 10, 11, and 8 shows the final change probability	1029
976	map (i.e., difference image) correspond to different SOTA	1030
977	methods on OSCD dataset.	1031
978		1032
979		1033
980		1034
981		1035
982		1036
983	<i>Continue on next page ...</i>	1037
984		1038
985		1039
986		1040
987		1041
988		1042
989		1043
990		1044
991		1045
992		1046
993		1047
994		1048
995		1049
996		1050
997		1051
998		1052
999		1053
1000		1054
1001		1055
1002		1056
1003		1057
1004		1058
1005		1059
1006		1060
1007		1061
1008		1062
1009		1063
1010		1064
1011		1065
1012		1066
1013		1067
1014		1068
1015		1069
1016		1070
1017		1071
1018		1072
1019		1073
1020		1074
1021		1075
1022		1076
1023		1077
1024		1078
1025		1079

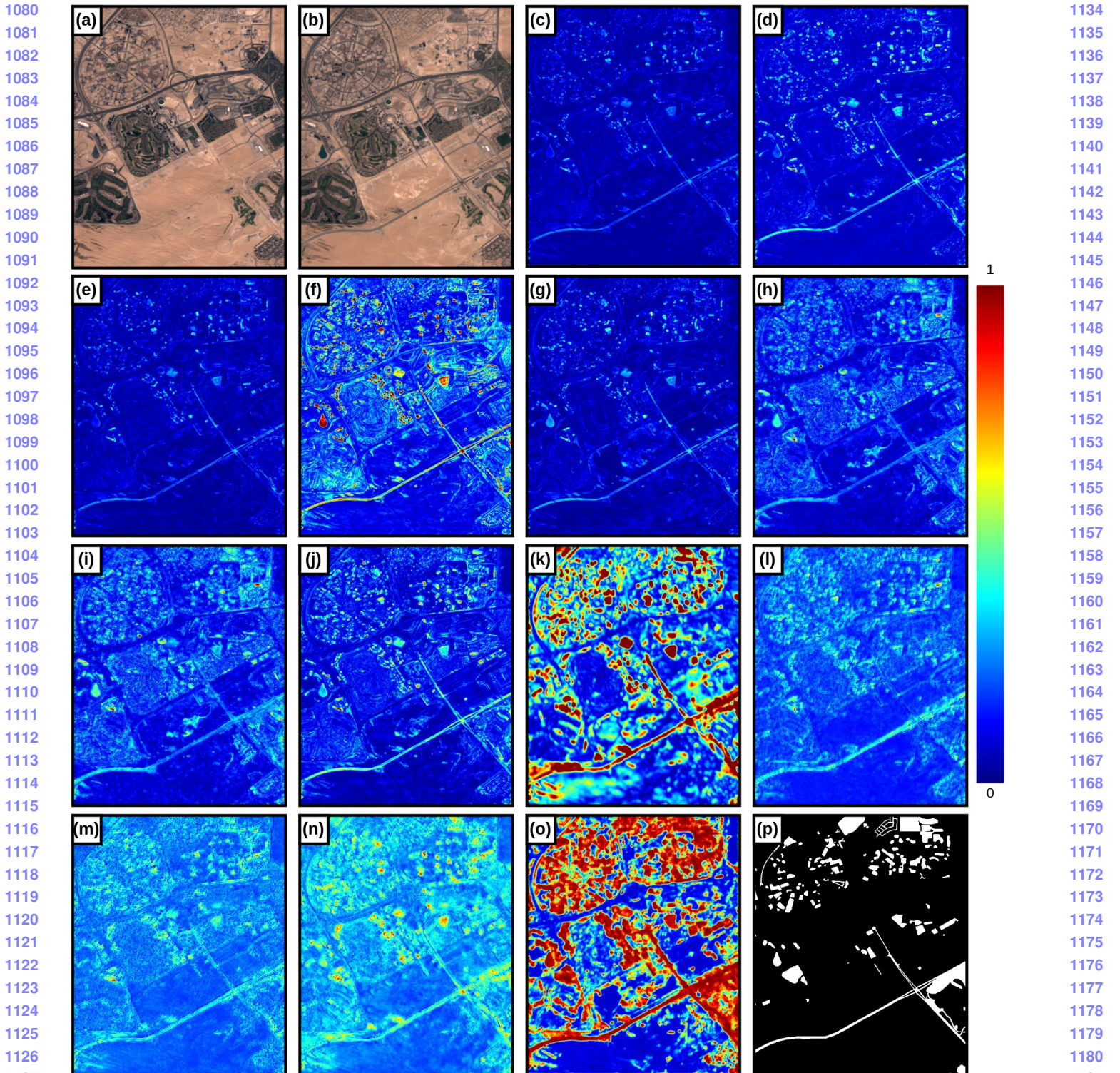


Figure 9. Change probability map (i.e., difference image) of different CD methods for dubai image pair in OSCD dataset. (a) Pre-change image. (b) Post-change image. (c) CVA. (d) DPCA. (e) ImageDiff. (f) ImageRatio. (g) ImageRegr. (h) IRMAD. (i) MAD. (j) PCDA. (k) DeepCVA. (l) UNet. (m) SeCo-Rand. (n) SeCo-Pre. (o) TTT-CD (ours). (p) Groud-truth change mask.

1131

1132

1133

1182

1183

1184

1185

1186

1187

1188  
1189  
1190  
1191  
1192  
1193  
1194  
1195  
1196  
1197  
1198  
1199  
1200

1201  
1202  
1203  
1204  
1205  
1206  
1207  
1208  
1209  
1210  
1211  
1212

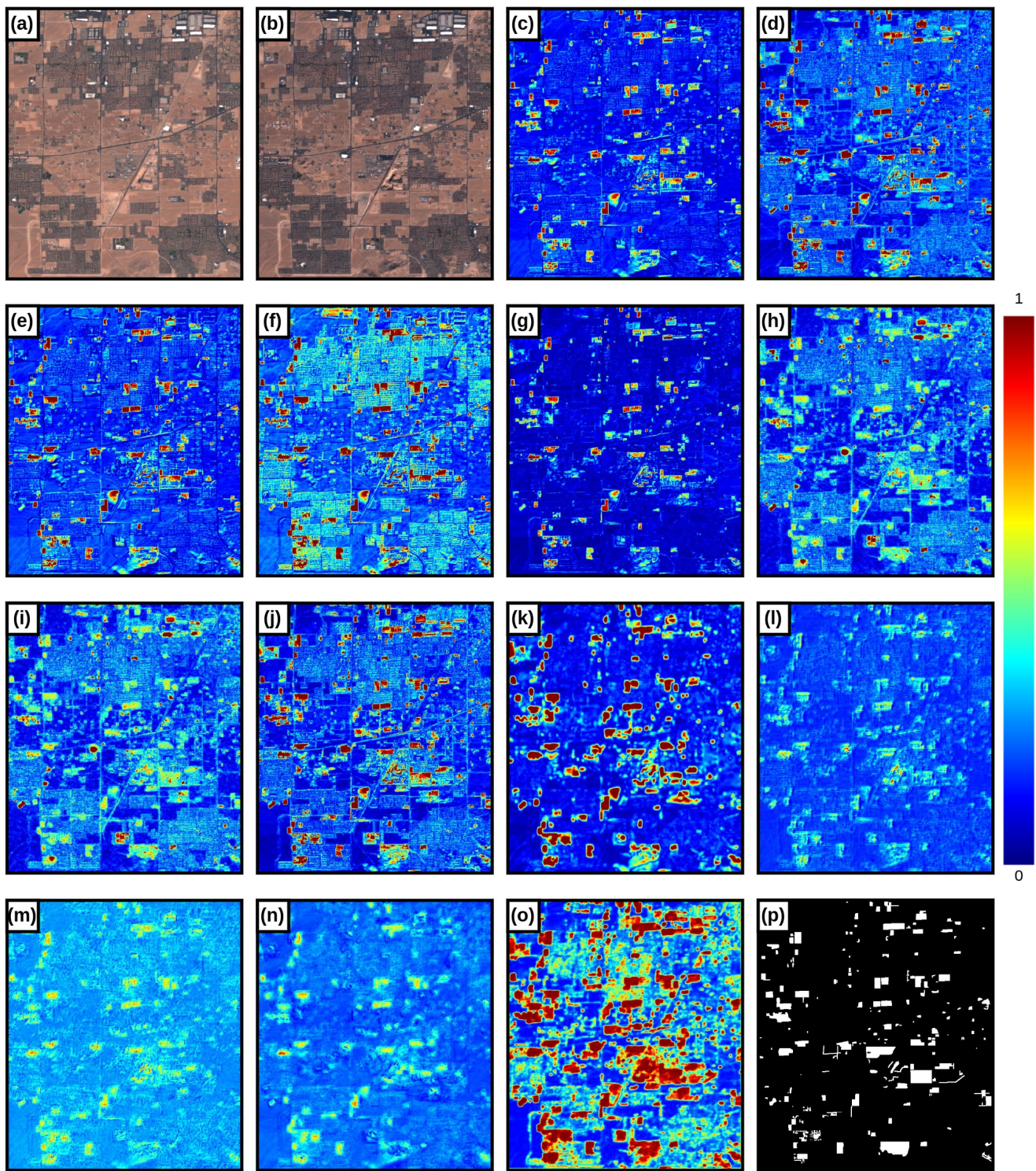
1213  
1214  
1215  
1216  
1217  
1218  
1219  
1220  
1221  
1222  
1223  
1224

1225  
1226  
1227  
1228  
1229  
1230  
1231  
1232  
1233  
1234  
1235  
1236

1237 Figure 10. Change probability map (i.e., difference image) of different CD methods for lasvegas image pair in OSCD dataset. (a) Pre-  
1238 change image. (b) Post-change image. (c) CVA. (d) DPCA. (e) ImageDiff. (f) ImageRatio. (g) ImageRegr. (h) IRMAD. (i) MAD. (j)  
1239 PCDA. (k) DeepCVA. (l) UNet. (m) SeCo-Rand. (n) SeCo-Pre. (o) TTT-CD (ours). (p) Groud-truth change mask.

1242  
1243  
1244  
1245  
1246  
1247  
1248  
1249  
1250  
1251  
1252  
1253  
1254  
1255  
1256  
1257  
1258  
1259  
1260  
1261  
1262  
1263  
1264  
1265  
1266  
1267  
1268  
1269  
1270  
1271  
1272  
1273  
1274  
1275  
1276  
1277  
1278

1279  
1280  
1281  
1282  
1283  
1284  
1285  
1286  
1287  
1288  
1289  
1290  
1291  
1292  
1293  
1294  
1295



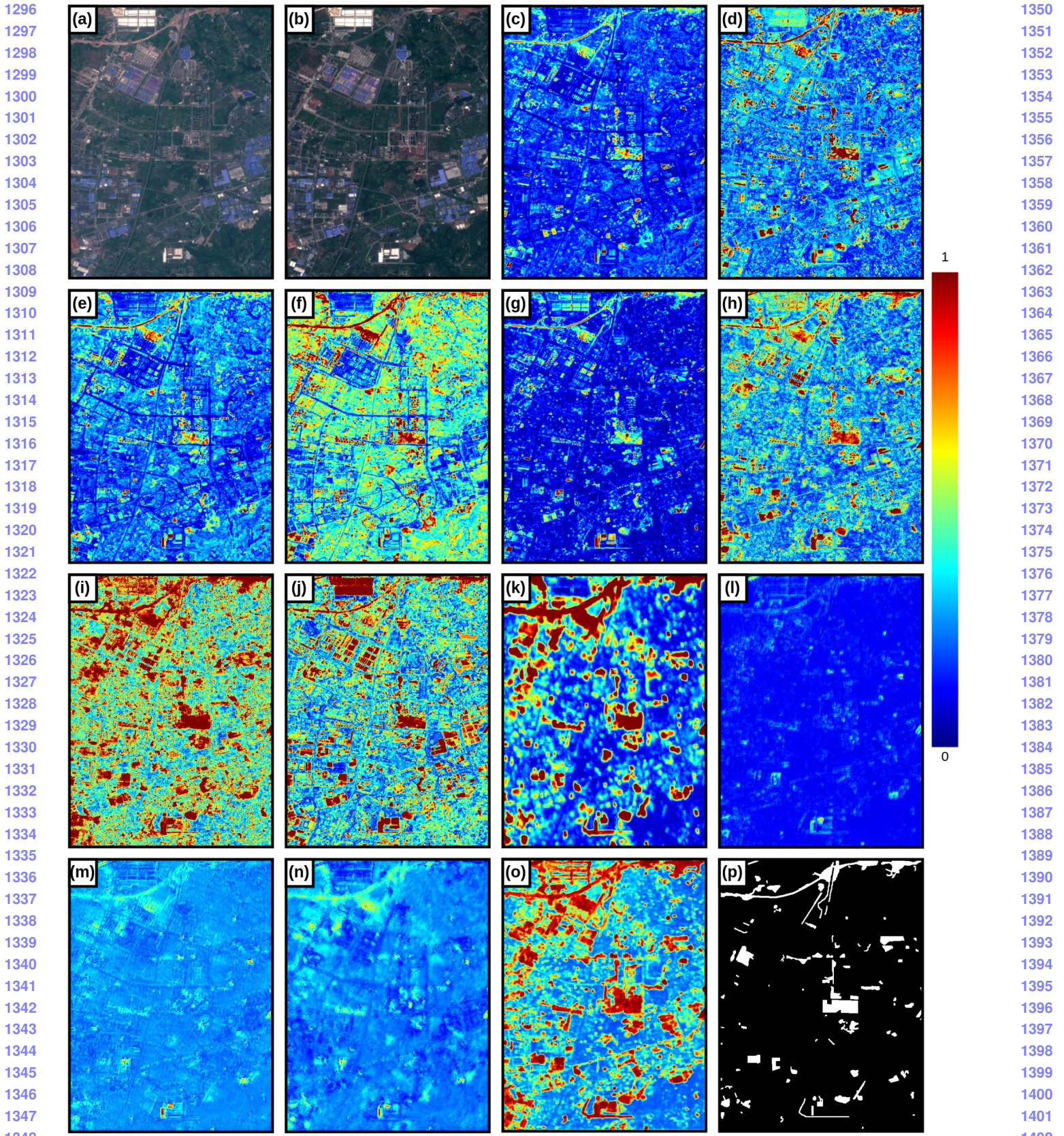


Figure 11. Change probability map (i.e., difference image) of different CD methods for chongqing image pair in OSCD dataset. (a) Pre-change image. (b) Post-change image. (c) CVA. (d) DPCA. (e) ImageDiff. (f) ImageRatio. (g) ImageRegr. (h) IRMAD. (i) MAD. (j) PCDA. (k) DeepCVA. (l) UNet. (m) SeCo-Rand. (n) SeCo-Pre. (o) TTT-CD (ours). (p) Groud-truth change mask.

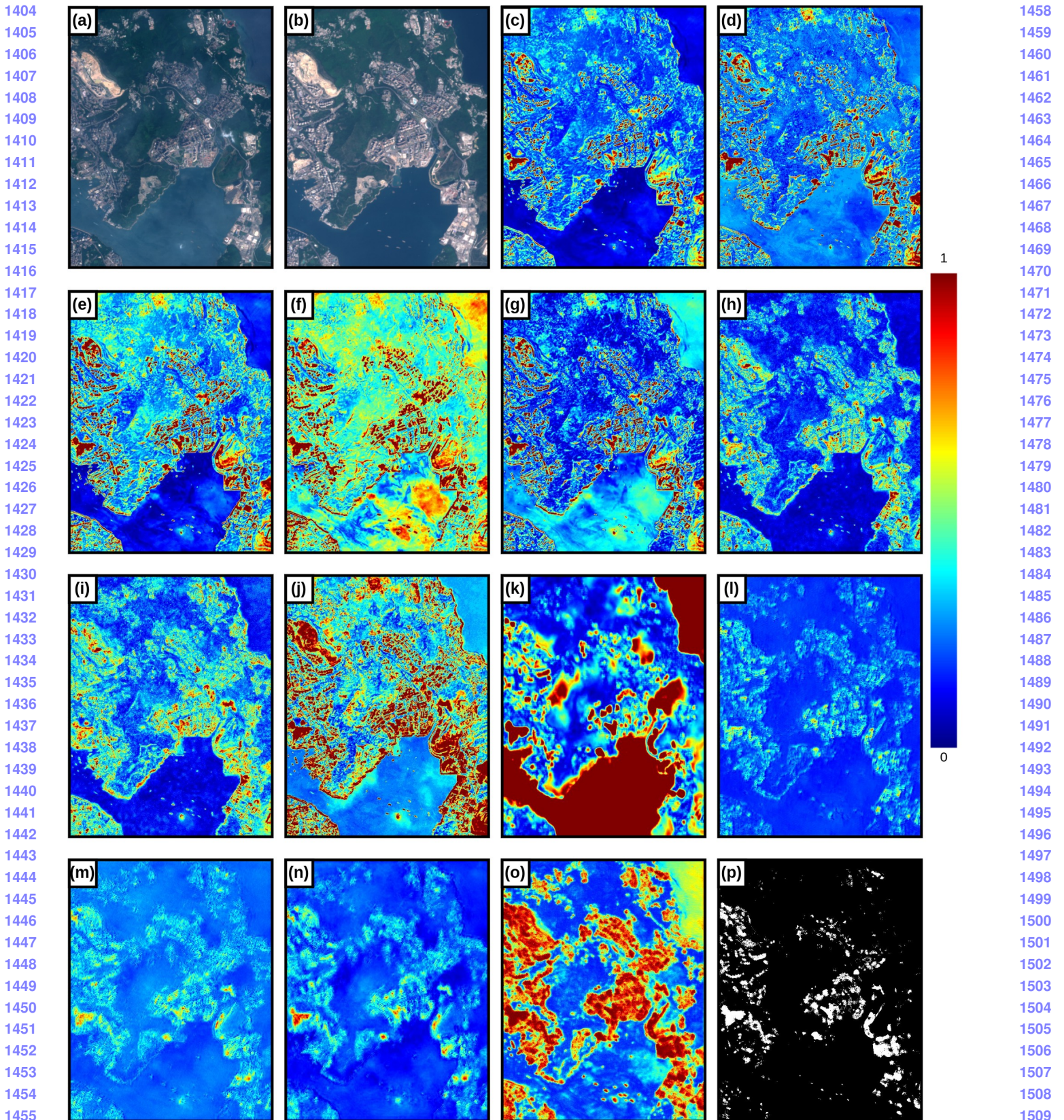


Figure 12. Change probability map (i.e., difference image) of different CD methods for hongkong image pair in OSCD dataset. (a) Pre-change image. (b) Post-change image. (c) CVA. (d) DPCA. (e) ImageDiff. (f) ImageRatio. (g) ImageRegr. (h) IRMAD. (i) MAD. (j) PCDA. (k) DeepCVA. (l) UNet. (m) SeCo-Rand. (n) SeCo-Pre. (o) TTT-CD (ours). (p) Groud-truth change mask.

1512	<b>4. Reproducing Results (Demo)</b>	1566
1513		1567
1514	1. Create a virtual conda environment using the provided	1568
1515	environment.yml (you may use: conda env create -f	1569
1516	environment.yml).	1570
1517		1571
1518	2. Once the environment is setup, open Demo_OSCD	1572
1519	from jupyter notebook and simply run the file.	1573
1520		1574
1521	3. GitHub repository will be made publically available	1575
1522	after the review process.	1576
1523		1577
1524		1578
1525		1579
1526		1580
1527		1581
1528		1582
1529		1583
1530		1584
1531		1585
1532		1586
1533		1587
1534		1588
1535		1589
1536		1590
1537		1591
1538		1592
1539		1593
1540		1594
1541		1595
1542		1596
1543		1597
1544		1598
1545		1599
1546		1600
1547		1601
1548		1602
1549		1603
1550		1604
1551		1605
1552		1606
1553		1607
1554		1608
1555		1609
1556		1610
1557		1611
1558		1612
1559		1613
1560		1614
1561		1615
1562		1616
1563		1617
1564		1618
1565		1619

1620	<b>References</b>	1674
1621		1675
1622	[1] Csaba Benedek and Tamás Szirányi. A mixed markov model	1676
1623	for change detection in aerial photos with large time differ-	1677
1624	ences. In <i>2008 19th International Conference on Pattern</i>	1678
1625	Recognition, pages 1–4. IEEE, 2008. <a href="#">2</a>	1679
1626	[2] Csaba Benedek and Tamás Szirányi. Change detection in op-	1680
1627	tical aerial images by a multilayer conditional mixed markov	1681
1628	model. <i>IEEE Transactions on Geoscience and Remote Sens-</i>	1682
1629	<i>ing</i> , 47(10):3416–3430, 2009. <a href="#">2</a>	1683
1630	[3] R. Caye Daudt, B. Le Saux, A. Boulch, and Y. Gousseau. Ur-	1684
1631	bani change detection for multispectral earth observation using	1685
1632	convolutional neural networks. In <i>IEEE International Geo-</i>	1686
1633	<i>science and Remote Sensing Symposium (IGARSS)</i> , July 2018.	1687
1634	<a href="#">1</a> , <a href="#">2</a>	1688
1635		1689
1636		1690
1637		1691
1638		1692
1639		1693
1640		1694
1641		1695
1642		1696
1643		1697
1644		1698
1645		1699
1646		1700
1647		1701
1648		1702
1649		1703
1650		1704
1651		1705
1652		1706
1653		1707
1654		1708
1655		1709
1656		1710
1657		1711
1658		1712
1659		1713
1660		1714
1661		1715
1662		1716
1663		1717
1664		1718
1665		1719
1666		1720
1667		1721
1668		1722
1669		1723
1670		1724
1671		1725
1672		1726
1673		1727